Journal of Hazardous Materials 184 (2010) 684–689

Contents lists available at ScienceDirect

Journal of Hazardous Materials

journal homepage: www.elsevier.com/locate/jhazmat

Fabrication of nanospinel $ZnCr_2O_4$ using sol–gel method and its application on removal of azo dye from aqueous solution

Mohammad Yazdanbakhsh[a,*], Iman Khosravi[a], Elaheh K. Goharshadi[a,b], Abbas Youssefi[c]

[a] Department of Chemistry, Faculty of Sciences, Ferdowsi University of Mashhad, Mashhad 91799, Iran
[b] Center of Nano Research, Ferdowsi University of Mashhad, Mashhad 91799, Iran
[c] Par-e-Tavous Research Institute, Mashhad 91000, Iran

ARTICLE INFO

Article history:
Received 29 March 2010
Received in revised form 9 August 2010
Accepted 22 August 2010
Available online 21 September 2010

Keywords:
Nanostructures
$ZnCr_2O_4$
Sol–gel growth
Azo-dye removal
Reactive blue 5

ABSTRACT

For the first time, nanoparticles of zinc chromite, spinel $ZnCr_2O_4$ have been fabricated by the thermal decomposition of Zn–Cr gel prepared by sol–gel method in the presence of oxalic acid as a chelating agent. It was shown that the well-crystallized spinel structure is formed after calcination at 450 °C. The nanospinel has been characterized by differential thermal analysis (DTA), X-ray powder diffraction (XRD), infrared spectroscopy (IR), and transmission electron microscope (TEM). The average particle size is approximately 13 nm according to the TEM image. The nanoparticles of zinc chromites showed excellent adsorption properties towards reactive dye, reactive blue 5 (RB5). The adsorption studies have been carried out for contact time, different pH values, different temperatures, and adsorbent doses. The investigation of removal kinetics of RB5 indicates that the removal process obeys the rate of second-order kinetic equation. The results indicate that the Langmuir adsorption isotherm fitted the data better than the Freundlich. Also, the photocatalytic degradation of RB5 using spinel $ZnCr_2O_4$ under UV irradiation at pH = 1 has been also examined. The results showed that the degradation of RB5 dye follows merely an adsorption process.

1. Introduction

Spinel compounds have a general formula AB_2O_4, in which the A-site is tetrahedrally coordinated and generally occupied by divalent cations (Mg, Mn, Ni, and Zn) and the B-site is octahedrally coordinated and occupied by trivalent cations (Al, Cr, and Fe). In solid-state science, oxides with spinel structures are some of the most studied compounds due to their wide range of applications. The structure of spinel oxide is responsible for a variety of interesting properties. Determination of cation distribution is of considerable relevance because the theoretical interpretation of the chemical and physical properties of these compounds depends on this distribution [1].

Spinels such as $ZnCr_2O_4$ containing transition metal ions can act as the efficient catalysts in the number of heterogeneous chemical processes such as CO oxidation [2], catalytic combustion of hydrocarbons [3], reduction of several organic molecules [4], and sensing properties [5]. The nanoparticles $ZnCr_2O_4$ have been synthesized by various methods including mechanical activation [6], high-temperature solid-state reaction [7], microemulsion method [8], solution method [9], and spray pyrolysis [10].

The most general method for preparing spinels involves solid-state reaction of the parent metal oxides which are mechanically mixed in the form of finely divided powders [11]. However, for completing the reaction, a temperature of about 1100 °C for several days is needed [12]. The disadvantages of solid-state routes such as inhomogeneity, lack of stoichiometry control, and larger particle size are avoided when the material is synthesized using a solution-based method. The main advantage is the molecular level mixing which facilitates the formation of polycrystalline homogeneous particles with improved properties.

Dye effluents from textile industries and photographic industries are becoming a serious environmental problem because of their toxicity, unacceptable color, high chemical oxygen demand content, and biological degradation [13]. Various treatment techniques and processes have been used to remove the pollutants from contaminated water. Among all the approaches proposed, adsorption is one of the most popular methods which are currently considered as an effective, efficient, and economic method for water purification [14].

Wu et al. [15] evaluated the effectiveness of magnetic ferrite $CuFe_2O_4$ powder as an adsorbent/catalyst material for the removal of azo-dye acid red B (ARB). They showed magnetic $CuFe_2O_4$ pow-

* Corresponding author. Tel.: +98 5118797022; fax: +98 5118796416.
E-mail address: myazdan@um.ac.ir (M. Yazdanbakhsh).

0304-3894/$ – see front matter © 2010 Elsevier B.V. All rights reserved.
doi:10.1016/j.jhazmat.2010.08.092

der possesses the excellent adsorptive properties towards azo-dye ARB at pH < 5.5.

Lou et al. synthesized Zn_2SnO_4 nanometer material with the structure of spinel-type one-step by the hydrothermal process under mild reaction conditions [16]. The samples were used as catalysts for the photodegradation of water-soluble dyes, such as reactive dyes K-NR, B-RN, and B-GFF. Their results showed that $SnZn_2$–O_4 nanocrystal is a promising material for photodegradating water soluble dyes due to its high photocatalytic activity.

Gao et al. synthesized magnetic mesoporous spinel $NiFe_2O_4$ of high surface area by a facile oxalate decomposition process [17]. The mesoporous material showed good adsorptive property for acid orange 7 (AO7) and it can be used as a magnetically separately adsorbent to treat AO7 contained wastewater.

Photocatalytic degradation processes have been widely applied as techniques of destruction of organic pollutants in wastewater and effluents [18].

The present study focuses on the preparation of $ZnCr_2O_4$ nanoparticles via the sol–gel method, characterization the nanoparticles, and investigation into its efficiency as an adsorbent for the removal of azo dye, reactive blue 5, from an aqueous solution. For removal investigation, the adsorption studies were carried out for contact time, different pH values, different temperatures, and adsorbent doses. Two kinetic models were also analyzed for the removal of RB5 on $ZnCr_2O_4$ nanoparticles. The last aim of the present study is to investigate the photocatalytic decomposition of RB5 in water over $ZnCr_2O_4$ nanoparticles.

2. Experimental procedure

2.1. Preparation of $ZnCr_2O_4$ powders

The appropriate amounts of starting materials $Cr(NO_3)_2{\cdot}9H_2O$ (0.1 M, 99.0%) and $Zn(NO_3)_2{\cdot}4H_2O$ (0.05 M, 99.0%) were dissolved in ethanol (95.0%) and then slowly ethanol solution of oxalic acid (0.15 M, 99.8%) was added at room temperature under constant magnetic stirring. The mixture was stirred for 18 h and then evaporated at 70 °C for 2 h under constant stirring which led to the formation of a sol. The sol was heated at 120 °C in baking oven until gel was formed. The gel was ground in an agate mortar and turned into powder. The powder was slowly heated at 250 °C for 2 h to decompose the organic materials completely and then it was calcined at 450 °C for 4 h for obtaining the well-crystallized spinel.

The nanoparticles were characterized by XRD employing a scanning rate of 0.02 s^{-1} in a 2θ range from 0° to 70°, using a Xí pert, 200, Philips, the Netherlands, equipped with Cu Kα radiation. The data were analyzed using JCPDS standards.

The morphology and dimension of the nanoparticles were observed by transmission electron microscope which was taken on a LEO 912 AB transmission electron microscope using an accelerating voltage of 120 kV. Samples for TEM were prepared by sonicating small amounts of the powder in 5 mL of ethanol for 30 min and then depositing a few drops of the suspension on a holey carbon grid.

The thermal behavior of the precursor was studied by differential thermal analysis in air at a heating rate of 10 °C min^{-1} using a NETZSCH.

Infrared spectra were recorded in the 250–4000 cm^{-1} range (KBr pellets) on thermo Nicollet Nexus 870 FT-IR spectrometer equipped with DTGS polyethylene detector and solid subtract beam splitter IR spectrometer.

2.2. Dye removal experiments

The commercial color index (CI) reactive dye (reactive blue 5, molecular weight = 774.16) was generously provided by Arzoo Textile Mills, Faisalabad, Pakistan which was used without further purification (Fig. 1).

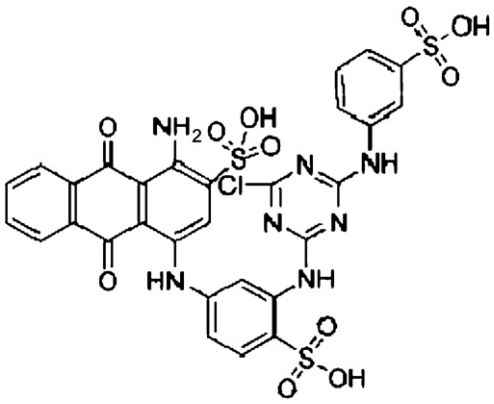

Fig. 1. Chemical structure of reactive blue 5 (RB5) dye.

The synthetic dye solution was distributed into different flasks (1 L capacity) and pH was adjusted with the help of pH meter (Metrohm 620, Swiss made). The initial pH of the sample was set by using dilute sodium hydroxide (1 M) or hydrochloric acid (1 M).

The initial dye concentration in each sample was 50 mg L^{-1} after adding 0.05 g of $ZnCr_2O_4$ in 50 mL of the sample. The removal pollution experiments were conducted at 25 °C and the pH values 1, 2, 7, and 11.

Each experiment was conducted for 1 h and samples were drawn at time intervals of 1, 5, 10, 20, 30, 40, 50, and 60 min for measuring the dye decomposition. The absorbance of the solution at 599 nm (UNICO 2800) with time has been measured to monitor the RB5 concentration. All experiments have been performed in duplicate to guarantee the reproducibility of the results. The mean of two measurements has been reported. All experiments have been performed at room temperature.

2.3. Photocatalytic activity experiments

The photocatalytic activity of $ZnCr_2O_4$ was evaluated by the degradation of azo dye, RB5. In a typical experiment, a 50 mL of dye solution 50 mg L^{-1} and a 0.05 g of photocatalyst $ZnCr_2O_4$ were mixed using a magnetic stirrer. After a period of time in the dark, the solution was irradiated. The light source was the mercury lamp (λ_{max} = 365 nm) with a power of 300 W. The samples of reaction mixture were taken from the reactor, at appropriate time intervals, in order to monitor the dye concentration in the solution. The solution was analyzed by the UV–vis method using UNICO 2800 spectrometer. The concentration of RB5 in the samples was calculated using calibration curve. The temperature of all experiments was carried out at 25 °C.

3. Results and discussion

3.1. Thermal analysis

Fig. 2 shows the DTA curve of the $ZnCr_2O_4$ gel precursor obtained by the sol–gel method. The DTA curve shows a large endothermic peak around 150 °C which is assigned to the evaporation of ethanol. The exothermic peak around 270 °C might be due to the combustion of the organic compounds such as oxalic acid and residual ethanol. The small exothermic peak at 370 °C can be attributed to the decomposition of nitrate which decomposes completely around 420 °C and results a large exothermic peak. No obvious change was observed above 470 °C. Hence, it is plausible to conclude that the lowest calcination temperature is about 450 °C.

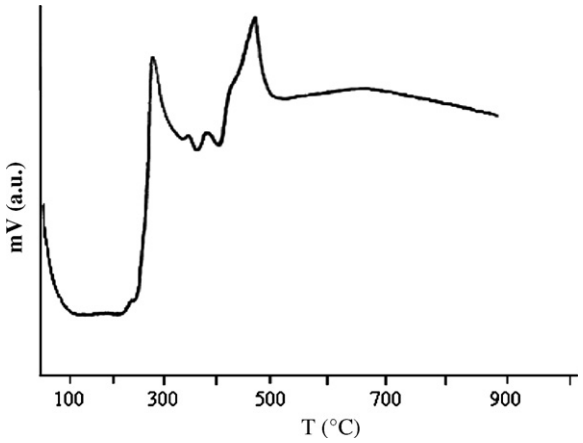

Fig. 2. DTA curve of the $ZnCr_2O_4$ precursors obtained by the oxalic acid-assisted sol–gel method.

3.2. X-ray diffraction studies

Fig. 3 shows the X-ray diffraction patterns using CuKα radiation from the spinel-type $ZnCr_2O_4$ formed when the gel was calcined at 450 and 700 °C for 4 h. The diffraction peaks at 2θ angels appeared 30.41°, 35.75°, 37.44°, 43.49°, 53.91°, 57.35°, and 62.95° can be assigned to scattering from the (2 2 0), (3 1 1), (2 2 2), (4 0 0), (4 2 2), (5 1 1), and (4 4 0) planes of the spinel crystal lattice, respectively.

The peaks of XRD confirm clearly that the phases belong to $ZnCr_2O_4$ and match well with the phase reported in the powder diffraction database [19]. The data of XRD shows $ZnCr_2O_4$ crystallizes in a cubic phase with $a = 8.2800$ Å, and space group *Fd3m* ($Z = 8$).

The crystallite sizes were calculated from the XRD peak broadening of the (3 1 1) peak using the Scherer's formula:

$$D_{hkl} = \frac{0.9\lambda}{\beta_{hkl} \cos \theta_{hkl}} \quad (1)$$

where D_{hkl} is the particle size perpendicular to the normal line of ($h\,k\,l$) plane, β_{hkl} is the full width at half maximum, θ_{hkl} is the Bragg angle of ($h\,k\,l$) peak, and λ is the wavelength of X-ray.

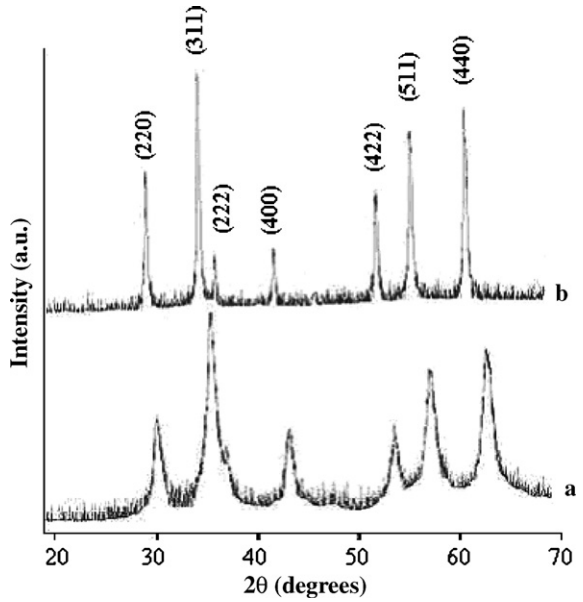

Fig. 3. XRD patterns of the $ZnCr_2O_4$ powders sintered at (a) 450 °C and (b) 700 °C.

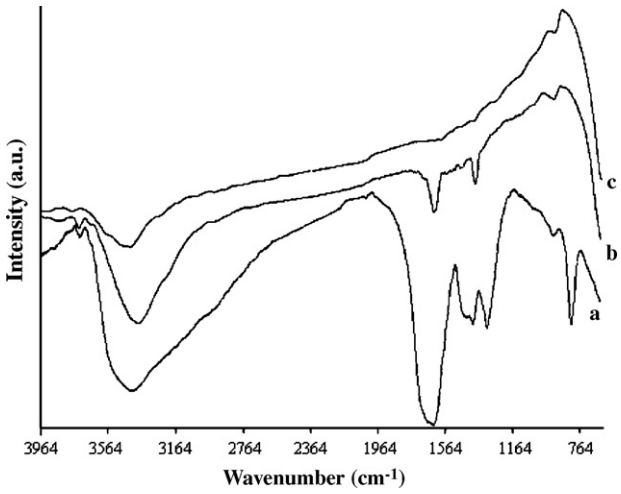

Fig. 4. IR spectra of $ZnCr_2O_4$ (a) precursor, (b) the calcined powders at 250 °C, and (c) at 450 °C.

The particle sizes of $ZnCr_2O_4$ nanoparticles calcinated at 450 and 700 °C are 13 and 40 nm, respectively. The peak intensity of the diffraction peaks and crystalline size increases with increasing the calcination temperature [20].

3.3. IR spectra of dried gel and annealed particles

The chemical and structural changes that take place during heating treatment can be monitored by a spectroscopic analysis. Fig. 4 shows the IR spectra of the dried gel and the annealed particles. The dried gel shows the characteristic bands at about 3390, 1633, and 1384 cm^{-1} corresponding to the stretching mode of O–H group in the free and absorbed ethanol, H–O–H bending vibration [21] of the residual ethanol, and the anti-symmetric NO_3^- stretching vibration [22], respectively. When, the gel is annealed at 450 °C, the intensities of the bands corresponding to O–H group and NO_3^- decrease appreciably. It can be attributed to the loss of the residual ethanol and NO_3^- in the dried gel. There are two strong absorption bands at 599 and 490 cm^{-1} which can be attributed to $ZnCr_2O_4$ spinel [23].

The peaks at 599 and 490 cm^{-1} of the Far-IR spectrum (Fig. 5) are attributed to the stretching vibration mode of M–O for the tetrahedrally and octahedrally coordinated metal ion, respectively.

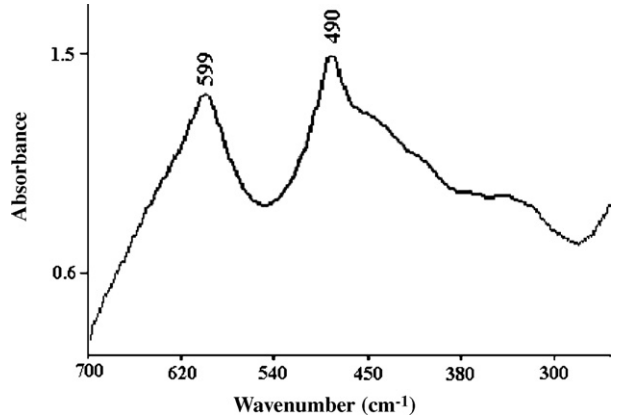

Fig. 5. Far-IR spectrum of $ZnCr_2O_4$.

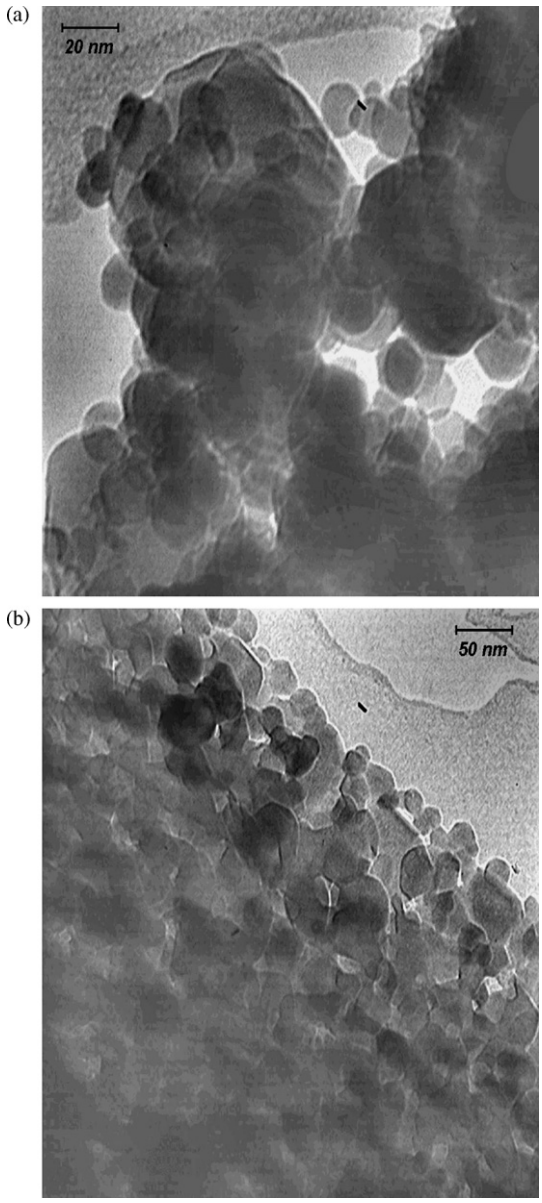

Fig. 6. (a and b) TEM micrograph of $ZnCr_2O_4$ nanoparticles obtained at 450 °C for 4 h with different magnifications.

3.4. Powder morphology

Fig. 6 shows the TEM images with different magnifications for the $ZnCr_2O_4$ nanoparticles prepared at 450 °C. As TEM images show the morphology of nanoparticles is homogeneous. The spinel nanoparticles consist of uniform quasi-spherical crystallites with an average size of 13 nm. This value is in agreement with the result achieved from XRD measurement.

3.5. Dye removal by $ZnCr_2O_4$ nanoparticles

The efficiency of prepared and characterized $ZnCr_2O_4$ nanoparticles has been investigated as an adsorbent for removal of RB5 from liquid solutions. The removal pollution experiments were conducted at 25 °C and the pH values of 1, 2, 7, and 11. The adsorption studies have been carried out for different pH values, contact time, different temperatures, and adsorbent doses which explained below.

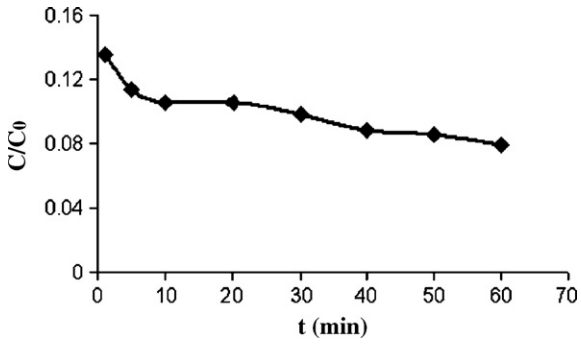

Fig. 7. Removal rate of RB5 on $ZnCr_2O_4$. Experimental conditions: mass of adsorbent, 0.05 g; initial dye concentration, 50 mg L^{-1}; volume of dye solution, 50 mL; temperature, 25 °C; and pH = 1.

3.5.1. The effect of pH

Since the solution pH is an important parameter on removal dye molecules [24], the initial pH of the solution has been changed in the range of 1–11. The results showed that the removal of RB5 is strongly dependent on pH.

The percentage of removal rate is defined as:

$$\text{Removal rate\%} = \frac{C_o - C(t)}{C_o} \times 100 \quad (2)$$

where C_o and $C(t)$ are the initial concentration and concentration of RB5 at time t, respectively. At pH = 1, the removal of RB5 above 91% was achieved. Hence, the removal of RB5 by $ZnCr_2O_4$ nanoparticles should be performed at pH = 1. This pH has been selected for investigating for the further experiments.

3.5.2. The effect of contact time

The effect of contact time on the removal of RB5 by $ZnCr_2O_4$ nanoparticles was illustrated in Fig. 7. This figure shows that the removal rate is very fast. The decrease in the concentration of RB5 with time is due to the adsorption of RB5 on $ZnCr_2O_4$ nanoparticles.

3.5.3. The effect of temperature

The effect of temperature on the RB5 removal onto $ZnCr_2O_4$ nanoparticles was carried out at 15, 25, 30, 35, and 40 °C. The temperature increasing from 15 to 25 °C led to an increase in the percentage of removal rate from 80.36 to 89.46, respectively. Consequently, it is plausible to say that the RB5 adsorption onto $ZnCr_2O_4$ nanoparticles may be a kinetically controlled process. Above 25 °C, increasing the temperature has no effect on the removal rate at all.

3.5.4. The effect of adsorbent concentration

The effect of adsorbent dosage of RB5 adsorption onto $ZnCr_2O_4$ nanoparticles was investigated. The results showed that as the adsorbent dose increases, the percentage removal of dye also increases. This is due to increase in binding sites in the adsorbent.

3.6. Chemical kinetic removal models

To find the suitable chemical removal model for describing the experimental kinetic data, the obtained data were fitted with the first and second-order models.

3.6.1. First-order kinetic model

The experimental data have been fitted with the following equation:

$$\ln \quad C(t) = \ln \quad C_o - k_1 t \quad (3)$$

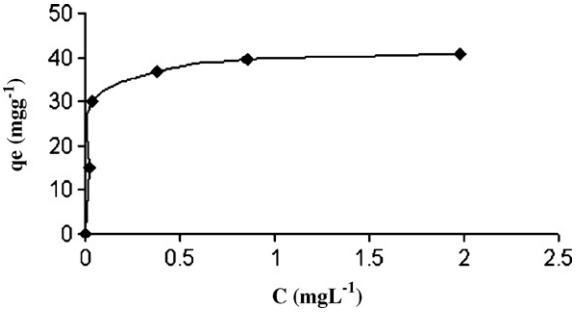

Fig. 8. Plots of q_e versus C_e for the adsorption of RB5 adsorption onto of $ZnCr_2O_4$. Experimental conditions: mass of adsorbent, 0.08 g; initial dye concentration, 25, 50, 75, 100, and 150 mg L^{-1}; volume of dye solution, 50 mL; temperature, 25 °C; and pH = 1.

where k_1 is the first-order rate constant and C_o stands for the initial RB5 concentration.

Since the correlation factor (R^2) is not higher than 0.98, the chemical kinetic removal model does not follow the first-order model.

3.6.2. Second-order kinetic model

The experimental data have been fitted with the second-order model:

$$\frac{1}{C(t)} = k_2 t + \frac{1}{C_o} \quad (4)$$

where k_2 is the second-order rate constant and it can be estimated from the slope of the curve of $1/C$ versus time. The correlation factor is 0.98 which is higher than that of the first-order model. Hence, our experimental data can be modeled by second-order kinetics. The value of the rate constant is 0.000353 M^{-1} min^{-1}.

3.7. Adsorption isotherms

The equilibrium adsorption isotherm model, which is the number of mg adsorbed per gram of adsorbent (q_e) versus the equilibrium concentration of adsorbate, C_e (Fig. 8), is fundamental in describing the interactive behavior between adsorbate and adsorbent. Analysis of isotherm data is so important to predict the adsorption capacity of the adsorbent, which is one of the main parameters required for designing the adsorption system [25].

The amount of dye adsorbed onto $ZnCr_2O_4$ nanoparticles has been calculated based on the following mass balance equation as:

$$q_e = \frac{V(C_o - C_e)}{m} \quad (5)$$

where q_e is the adsorption capacity (mg dye adsorbed onto the mass unit of $ZnCr_2O_4$, mg g^{-1}), V is the volume of the dye solution (L), C_o and C_e (mg L^{-1}) are initial and equilibrium dye concentrations, and m (g) is the mass of dry $ZnCr_2O_4$ added.

Several isotherm models have been developed to evaluate the equilibrium adsorption of compounds from solutions such as Langmuir, Freundlich, Redlich–Peterson, etc. The more common models used to investigate the adsorption isotherm are Langmuir and Freundlich. The experimental results of this study have been fitted with theses two models.

The linearized form of the Langmuir isotherm, assuming monolayer adsorption on a homogeneous adsorbent surface, is expressed as follows [26]:

$$\frac{C_e}{q_e} = \frac{1}{bq_{max}} + \frac{C_e}{q_{max}} \quad (6)$$

where the q_{max} (mg g^{-1}) is the surface concentration at monolayer coverage which illustrates the maximum value of q_e and it can be attained as C_e is maximized. The b parameter is a coefficient related to the energy of adsorption and increases with increasing strength of the adsorption bond. Values of q_{max} and b are determined from the linear regression plot of (C_e/q_e) versus C_e. The parameters of the Langmuir equation in this work, namely q_{max} and b are 41.322 mg g^{-1} and 0.747 L mg^{-1}, respectively.

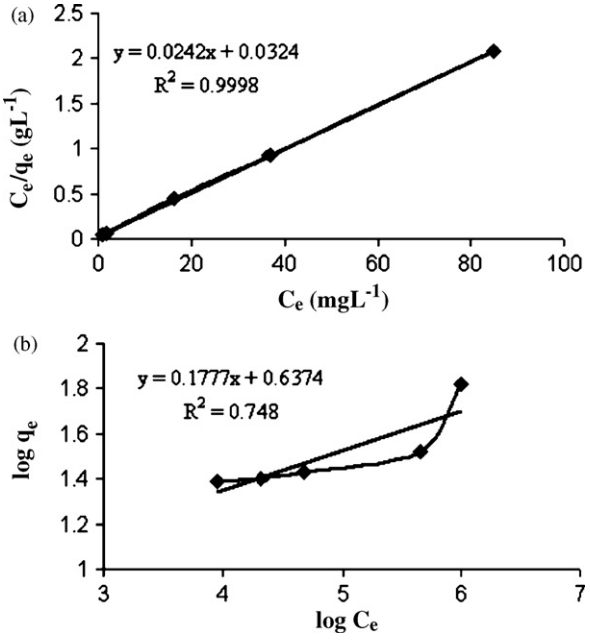

Fig. 9. The plot of linearized form of (a) the Langmuir isotherm (b) the Freundlich isotherm. Experimental conditions: mass of adsorbent, 0.08 g; initial dye concentration, 25, 50, 75, 100, 150 mg L^{-1}; volume of dye solution, 50 mL; temperature, 25 °C; and pH = 1.

The Freundlich equation [27] is expressed as follows in its linearized form:

$$\log\ q_e = \log\ K_F + \frac{1}{n}\ \log\ C_e \quad (7)$$

where K_F and n are constants of the Freundlich equation. The constant K_F represents the capacity of the adsorbent for the adsorbate. n is related to the adsorption distribution. A linear regression plot of $\log q_e$ versus $\log C_e$ gives the K_F and n values.

The value of correlation coefficient (R^2) for Langmuir isotherm is greater than that of the Freundlich isotherm for the adsorption of the dye (Fig. 9a and b). This indicates that Langmuir model can describe the adsorption of RB5 on $ZnCr_2O_4$ nanoparticles better than the Freundlich model. This shows that the adsorption occurs as the monolayer dye adsorbs onto the homogenous adsorbent surface.

3.8. Photocatalytic activity measurement

Three comparison experiments were carried out under the same conditions, one in the presence of $ZnCr_2O_4$ and UV irradiation, second without $ZnCr_2O_4$, and third in the dark (Table 1). Since some dyes are degraded by direct UV irradiation, it should be examined to what extent RB5 is photolyzed if no photocatalyst was used. In the

Table 1
The percentage removal rate of RB5 solution at different conditions.

t (min)	1	5	10	20
$ZnCr_2O_4$ + UV irradiation	90	92	94	96
$ZnCr_2O_4$	86.5	88.5	89	90
UV irradiation	3	5	7	13

absence of the catalyst, RB5 was photolyzed by direct UV radiation only up to 13% in 20 min. It is obvious that simultaneous utilization of UV irradiation with $ZnCr_2O_4$ nanoparticles could increase the decolorization rate of RB5 so that 90% of RB5 is removed within 1 min. In the presence of catalyst, $ZnCr_2O_4$, without irradiation, the dye concentration decreases quickly at starting, and then reaches a saturation value, which is due to the adsorption of dye molecule on the catalyst. Hence, nanoparticles of $ZnCr_2O_4$ cannot act as photocatalyst for the degradation of RB5 in an aqueous solution. The degradation follows merely an adsorption process.

4. Conclusions

Spinel $ZnCr_2O_4$ nanoparticles have been fabricated using by the thermal decomposition of Zn–Cr gel prepared by sol–gel method in the presence of oxalic acid as a chelating agent. The particle size of nanoparticles is so small in comparison with those prepared by conventional methods [28].

The XRD and TEM reveal that the $ZnCr_2O_4$ nanoparticles prepared by calcinating the gel precursor at 450 °C for 4 h have good crystallinity with fine cubic spinel structure. The nanoparticles exhibit a regular morphology with homogeneous particle size distribution. The IR spectra also confirmed the structure of prepared nanoparticles.

The adsorption studies have been carried out for contact time, different pH values, different temperatures, and adsorbent doses separately. $ZnCr_2O_4$ nanoparticles have been also proven to removal azo-dye RB5 at pH = 1 effectively. The results show the $ZnCr_2O_4$ nanoparticles can effectively remove high concentrations of RB5 dye molecules.

The second-order kinetic model is more successful in representing the experimental data for the removal of RB5 on $ZnCr_2O_4$ nanoparticles. The isotherm modeling reveals that Langmuir equation describes the adsorption of RB5 dye onto the $ZnCr_2O_4$ better than the Freundlich model.

Experimental results of the photocatalytic decolorization of the azo-dye RB5 using $ZnCr_2O_4$ reveal that the decolorization can be achieved by an adsorption process.

Acknowledgments

The authors acknowledge the support of Ferdowsi University of Mashhad for this project (P438) and are grateful to Dr. F. Tayyari and N. Ghows for their help. We also acknowledge R. Pesian and N. Hashemian for taking TEM images at the central lab of Ferdowsi University of Mashhad.

References

[1] S. Lv, X. Chen, Y. Ye, S. Yin, J. Cheng, M. Xia, Rice hull/$MnFe_2O_4$ composite: preparation, characterization and its rapid microwave-assisted COD removal for organic wastewater, J. Hazard. Mater. 171 (2009) 634–639.
[2] J. Ghose, R.C. Murthy, Activity of Cu^{2+} ions on the tetrahedral and octahedral sites of spinel oxide catalysts for CO oxidation, J. Catal. 162 (1996) 359–360.
[3] N. Guilhaume, M. Primet, Catalytic combustion of methane: copper oxide supported on high-specific-area spinels synthesized by a sol–gel process, J. Chem. Soc. Faraday Trans. 90 (1994) 1541–1545.
[4] X. Wei, D. Chen, W. Tang, Preparation and characterization of the spinel oxide $ZnCo_2O_4$ obtained by sol–gel method, Mater. Chem. Phys. 103 (2007) 54–58.
[5] S. Pokhrel, B. Jeyaraj, K.S. Nagaraja, Humidity-sensing properties of $ZnCr_2O_4$–ZnO composites, Mater. Lett. 57 (2003) 3543–3548.
[6] Z.V. Marinkovic, L. Mancic, P. Vulic, O. Milosevic, The influence of mechanical activation on the stoichiometry and defect structure of a sintered ZnO–Cr_2O_3 system, Mater. Sci. Forum 453 (2004) 456–461.
[7] S. Levy, D. Diella, V. Pavese, A. Dapiaggi, M. Sani, A P–V equation of state, thermal expansion, and P–T stability of synthetic ($ZnCr_2O_4$ spinel), Am. Mineral. 90 (2005) 1157–1167.
[8] X. Niu, W. Du, W. Du, Preparation and gas sensing properties of ZnM_2O_4 (M = Fe, Co, Cr), Sens. Actuators B 99 (2004) 405–415.
[9] R.G. Chandran, K.C. Patil, A rapid method to prepare crystalline fine particle chromite powders, Mater. Lett. 12 (1992) 437–450.
[10] Z.V. Marinkovic, L. Mancic, R. Maric, O. Milosevic, Preparation of nanostructure Zn–Cr–O spinel powders by ultrasonic spray pyrolysis, J. Eur. Ceram. Soc. 21 (2001) 2051–2067.
[11] Z.V. Marinkovic, L. Mancic, P. Vulic, O. Milosevi, Microstructure characterization of mechanically activated ZnO–Cr_2O_3 system, J. Eur. Ceram. Soc. 25 (2005) 2081–2093.
[12] M. Bayhan, T. Hashemi, A.W. Brinkman, Sintering and humidity-sensitive behaviour of the $ZnCr_2O_4$–K_2CrO_4 ceramic system, J. Mater. Sci. 32 (1997) 6619–6623.
[13] M. Siddique, R. Farooq, A. Khalid, A. Farooq, Q. Mahmood, U. Farooq, I.A. Raja, S.F. Shaukat, Thermal-pressure-mediated hydrolysis of reactive blue 19 dye, J. Hazard. Mater. 172 (2009) 1007–1012.
[14] Q. Jiuhu, Research progress of novel adsorption processes in water purification: a review, J. Environ. Sci. 20 (2008) 1–32.
[15] R. Wu, J. Qu, H. He, Y. Yu, Removal of azo-dye acid red B (ARB) by adsorption and catalytic combustion using magnetic $CuFe_2O_4$ powder, Appl. Catal. B: Environ. 48 (2004) 49–56.
[16] X. Lou, X. Jia, J. Xu, S. Liu, Q. Gao, Hydrothermal synthesis, characterization and photocatalytic properties of Zn_2SnO_4 nanocrystal, Mater. Sci. Eng. A 432 (2006) 221–225.
[17] Z. Gao, F. Cui, S. Zeng, L. Guo, J. Shi, A high surface area superparamagnetic mesoporous spinel ferrite synthesized by a template-free approach and its adsorptive property, Micropor. Mesopor. Mater. 132 (2010) 188–195.
[18] T. Oppenlander, Photochemical Purification of Water and Air, Wiley-VCH, Weinheim, 2003.
[19] N. Kavaso_glu, M. Bayhan, Air moisture sensing properties of $ZnCr_2O_4$–K_2CrO_4 composites, Turk. J. Phys. 29 (2005) 249–255.
[20] L. Mancic, Z. Marinkovic, P. Vulic, C. Moral, O. Milosevic, Morphology, structure and nonstoichiometry of $ZnCr_2O_4$ nanophased power, Sensors 3 (2003) 415–423.
[21] M Sadakane, T. Horiuchi, N. Kato, C. Takahashi, W. Ueda, Facile preparation of three dimensionally ordered macroporous alumina, iron oxide, chromium oxide, manganese oxide, and their mixed-metal oxides with high porosity, Chem. Mater. 19 (2007) 5779–5785.
[22] C.V. Hernandez, O. Almanza, J.F. Jurado, EPR, μ-Raman and Crystallographic Properties of Spinel Type $ZnCr_2O_4$, J. Phys. Conf. Ser. 167 (2009) 012037.
[23] P. Parhi, V. Manivannan, Microwave metathetic approach for the synthesis and characterization of $ZnCr_2O_4$, J. Eur. Ceram. Soc. 28 (2008) 1665–1670.
[24] G. Bayramoglu, G. Celik, M.Y. Arica, Biosorption of reactive blue 4 dye by native and treated fungus *Phanerocheate chrysosporium*: batch and continuous flow system studies, J. Hazard. Mater. B. 137 (2006) 1689–1697.
[25] A. Afkhami, R. Moosavi, Adsorptive removal of Congo red, a carcinogenic textile dye, from aqueous solutions by magnetite nanoparticles, J. Hazard. Mater. 174 (2010) 398–403.
[26] I. Langmuir, The adsorption of gases on plane surfaces of glass, mica and platinum, J. Am. Chem. Soc. 40 (1918) 1361–1403.
[27] H.M.F. Freundlich, Over the adsorption in solution, Z. Phys. Chem. A. 57 (1906) 385–471.
[28] Y. Xue, S. Naher, F. Hata, H. Kaneko, H. Suzuki, Y. Kino, Low temperature X-ray diffraction study of $ZnCr_2O_4$ and $Ni_{0.5}Zn_{0.5}Cr_2O_4$, J. Low Temp. Phys. 151 (2008) 1193–1204.